

Cathodic inhibition and anomalous electrodeposition of Zn–Co alloys

Z.F. Lodhi^{a,*}, J.M.C. Mol^b, W.J. Hamer^a, H.A. Terryn^{a,c}, J.H.W. De Wit^{a,b}

^a *Netherlands Institute for Metals Research (NIMR), Mekelweg 2, 2600 GA Delft, The Netherlands*

^b *Delft University of Technology, Department of Materials Science & Engineering, Mekelweg 2, 2628 CD Delft, The Netherlands*

^c *Department of Metallurgy, Electrochemistry and Materials Science, Vrije Universiteit Brussel, Pleinlaan 2, B-1050 Brussels, Belgium*

Received 28 September 2006; received in revised form 16 February 2007; accepted 27 February 2007

Available online 4 March 2007

Abstract

The electrodeposition of Zn–Co alloys from chloride electrolytes was studied on steel substrate. Electrodeposition of Zn–Co alloys is usually divided into two potential regions, i.e. normal (positive to Zn deposition potential $E_{\text{Zn}}^0 = -1.05$ V versus SCE) and anomalous (negative to E_{Zn}^0). In order to elucidate the deposition mechanism a complementary approach was used based on the combination of various electrochemical techniques. The morphology of the deposits and elemental composition analysis were determined by using SEM/EDX. It was found that the presence of Zn^{2+} in electrolyte inhibited Co^{2+} and H^+ reductions in normal region. A critical potential was also noticed in the so-called normal deposition range above which a Co-enriched phase of Co–Zn alloy was favored and below that a severe mitigation to deposition occurred that was considered due to underpotential deposition (UPD) of Zn on the substrate and on active Co sites at either nucleation or growth stage. Beyond E_{Zn}^0 the deposition is considered anomalous due to the fact that Zn deposits preferentially compared to the more noble Co. This anomalism was explained by the faster deposition kinetics of Zn as compared to Co on steel and could be overcome by either increasing the $\text{Co}^{2+}/\text{Zn}^{2+}$ ratios in the electrolyte or by carrying out the deposition at higher temperature.

© 2007 Elsevier Ltd. All rights reserved.

Keywords: Anomalous electrodeposition; Zn–Co alloys; Underpotential deposition; Cathodic potentiodynamic polarization; Critical potential

1. Introduction

Zinc alloys with group eight metals (Ni, Co and Fe) have attracted a lot of interest because these alloys exhibit significantly higher corrosion resistance than pure zinc and have a potential to replace the banned cadmium coating. Electrodeposition of these alloys is classified as anomalous by Brenner [1] because the less noble zinc deposits preferentially under most plating conditions. This anomalism has yet to be explained. Several theories have been forwarded by various researchers [2–8], but the most widespread one, and subject of controversy, is the so-called ‘hydroxide suppression mechanism’ (HSM) [3–9]. This model, initially proposed by Dahm and Croll [2] for the Ni–Fe alloys, suggests that the discharge of more noble ions (i.e. Ni^{2+}) is hindered by the formation of $\text{Fe}(\text{OH})_2$ in respective electrolytes, due to local pH rise, on cathode surface and therefore inhibits the codeposition of Ni. Decroly and co-workers

[3,4] and Higashi et al. [5,6] proposed that the discharge of Co^{2+} ions is hindered in the same manner by the formation of $\text{Zn}(\text{OH})_2$ on cathode surface. Based on this theory, deposition conditions that can cause an increase in surface pH would enhance the anomalous codeposition. Tsuru et al. [9] have supported HSM theory by having a normal electrodeposition from a methanol bath and showed that anomalous behavior occurs when water is added to the electrolyte. Recently, the hydroxide oscillation concept was proposed [10], according to which the thickness of the hydroxide layer changes periodically and the hydrogen reduction and cobalt deposition takes place when the hydroxide layer is depleted. The pH increase due to the rapid H^+ reduction leads to the reformation of the layer and codeposition becomes anomalous. Higashi et al. [5] measured local pH in the vicinity of the electrode using an antimony micro-electrode during the Zn–Co electrodeposition process. With the initial electrolyte pH 5.0, they observed a rise in pH that might cause precipitation of $\text{Zn}(\text{OH})_2$ while inhibiting Co deposition. But other researchers [11–14] (with the initial pH less than 4.0) could not find a significant pH increase that could result in $\text{Zn}(\text{OH})_2$.

* Corresponding author. Tel.: +31 15 2783723; fax: +31 15 2786730.
E-mail address: z.f.lodhi@tudelft.nl (Z.F. Lodhi).

In contrast, several researchers have disagreed and objected to the HSM theory. Gomes and Valles [15] observed that an increase in the solution pH promote the normal codeposition of Zn–Co alloys while Chassaing and Miranda [16,17] found high Ni deposition at higher pH values during Zn–Ni electrodeposition in chloride and sulfate medium and suggest that the deposition of Ni is activated with an increase in solution pH of the Zn–Ni system, which is in contradiction with HSM. On the basis of impedance measurements during alloy deposition, they put forward that a mixed intermediate of $[\text{ZnNi}]_{\text{ad}}^+$ plays an important role in the preferential zinc deposition.

Some researchers [18–26] have investigated the deposition kinetics of Zn and iron group metals at various molar concentrations of electrolytes and reported the slower deposition kinetics of iron group metals being responsible for the anomalism.

Several others [26–31] suggested that the anomalous codeposition process is associated with the underpotential deposition (UPD) of the less noble metal on more noble metal substrate. Most of these researchers have tried to explain the anomalism with UPD in a region more negative to the zinc deposition potential. The term UPD refers to the phenomenon of deposition of less noble metal (i.e. zinc) on foreign substrates (i.e. steel) in the potential region more positive to the equilibrium potential of the less noble metal. The UPD of Zn has previously been reported [27–35] on several substrates, e.g. Fe, Co, Pt, Ag, Au, Cu and also steels. The UPD is usually considered limited to a monolayer but several layers of zinc deposits have also been reported [34–36]. Dogel and Freyland [34] has reported the deposition of three consecutive layers on the substrate and Fujuwara and Enomoto [36] has shown thick Zn-rich CuZn deposits in the underpotential region. Nicol and Philip [27] and Ohtsuka and Komori [29] suggested that the UPD of the less noble metal gives rise to preferential or anomalous deposition, but this model has not found much favor since anomalism occurs in the overpotential deposition region. This approach was found unable to explain how a thick (10–25 μm) Zn–Ni or Zn–Co alloys deposits (with higher zinc content) can be formed by the UPD mechanism at potentials more negative than the zinc equilibrium potential (i.e. in the overpotential region) [26].

In the presented work the electrodeposition mechanism of Zn, Co and Zn–Co alloys is studied by using cathodic potentiodynamic polarization, potentiostatic deposition and anodic stripping methods. The purpose is to elucidate various stages of anomalism and inhibition at various potentials and to explain which processes are responsible for it. Various existing theories are analyzed in this work to study which theory covers the results under the given operating conditions. Moreover, the effect of varying the composition and temperature of the electrolyte in overcoming anomalism is also studied.

2. Experimental

2.1. Material preparation

All coatings were electrodeposited from electrolytes prepared from chloride salts of respective metals. All the electrolytes were prepared from demineralised water and ana-

Table 1

Compositions of the various Zn, Co and ZnCo alloys electrolytes used for deposition

Electrolyte	ZnCl ₂ (g/L)	CoCl ₂ ·6H ₂ O (g/L)	Molar ratio Zn ²⁺ /Co ²⁺	%Co ²⁺
1	0	238	1.0	0
2	150	0	1.1	100
3	150	100	1.1/0.42	27.6
4	150	150	1.1/0.63	36.4
5	150	180	1.1/0.75	40
6	150	202	1.1/0.85	44
7	138	238	1.0/1.0	50

lytical grade chemicals. The deposition is done on high strength steel (AISI 4340) substrates. The chemical composition of AISI 4340 steel was 0.41% C, 0.73% Mn, 0.8% Cr, 1.74% Ni, 0.25% Mo and 0.25% Si (wt%). The surface area of the substrates was 1 cm². Before deposition the samples were thoroughly cleaned in alkaline solution (containing NaOH, Sodium gluconate, Na₃PO₄, Na₂CO₃ and alkaline surfactant) followed by anodic electrolytic cleaning in alkaline solution (containing NaOH, sodium gluconate and alkaline surfactant) for 3 min at 3 A/dm². After a thorough rinse with distilled water the samples were etched in 8% HCl for 3 min to neutralize the remnants of alkaline solution and to activate the surface. Finally, the substrates were rinsed again with water and alcohol and dried with air.

2.2. Electrolyte composition

The composition of blank solution was KCl 186 g/L (2.5 M), H₃BO₃ = 30 g/L (0.5 M) and NH₄Cl = 20 g/L (0.4 M). All electrodepositions, given in Table 1, were carried out at a constant bulk pH of 3.6 at 35 °C and the electrolytes were continuously stirred during deposition.

2.3. Potentiodynamic cathodic polarization measurement

Cathodic potentiodynamic polarization studies were carried out in a three-electrode cell. The cathode (high strength steel substrate) was immersed in aerated solutions (containing Zn, Co, ZnCo and blank solutions) as mentioned in the composition section above. Saturated Calomel Electrode (SCE) was used as an external reference electrode and a Luggin capillary was used to keep the reference electrode as close as possible to overcome the ohmic resistance. A platinum mesh anode was used to complete the cell. A Solarton 1286 computer controlled potentiostat was used to apply the potential ranging from –0.4 V to –1.5 V at a scan rate of 1 mV/s and the resulting current density was recorded.

2.4. Potentiostatic electrodeposition

Potentiostatic depositions of Zn, Co and Zn–Co alloy were carried out at –0.78 V, –0.90 V and –1.10 V onto steel substrates for 3–5 min. The current was monitored and recorded during deposition. The potentiostatic cathodic measurements were also conducted in a three-electrode cell, provided with steel

disc of an area 1 cm^2 , as cathode. A platinum mesh was used as anode and a saturated calomel electrode as a reference electrode. The potential application to the working electrode and the current measurement was done via Solartron 1286 computer controlled potentiostat.

2.5. Anodic stripping technique

Anodic stripping analysis is employed effectively for the in situ characterization of the electrodeposition process and products of the potentiostatically obtained electrodeposits on steel substrate. For anodic stripping the potentiostatic deposition was carried out for a few seconds (time was adjusted with applied potential) in order to obtain a thin deposit. The purpose of these measurements was to perform a qualitative analysis and not a quantitative one. The analysis was performed right after the potentiostatic depositions, in situ, without removing the sample from the respective electrolytes. The set up is the same as mentioned above for potentiostatic deposition. The stripping was set to start from the deposition potential and was done at a scan rate of 10 mV/s .

2.6. Microscopic and composition analysis

A JEOL 6400 scanning electron microscope (SEM) was used to examine the surface morphology of the coatings after electrodeposition. The elemental composition of the electrodeposits was determined with energy dispersive X-rays (EDX) working at $15\text{--}20 \text{ kV}$ in association with SEM.

3. Results

3.1. Cathodic potentiodynamic polarization curves

Fig. 1 shows the cathodic potentiodynamic polarization curves for blank electrolyte (in which no Zn^{2+} or Co^{2+} ions are present) at 25°C and rest of the operating conditions are same

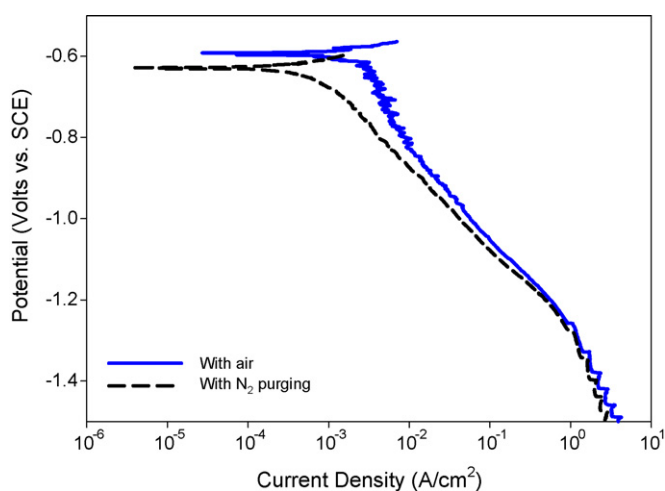


Fig. 1. Cathodic potentiodynamic polarization curves on steel substrate. The two curves elucidate the contribution of hydrogen and oxygen reduction (with and without N_2 purging) during the polarization. The polarization is carried out at 25°C , $\text{pH } 3.5$ and at a scan rate of 1 mV/s .

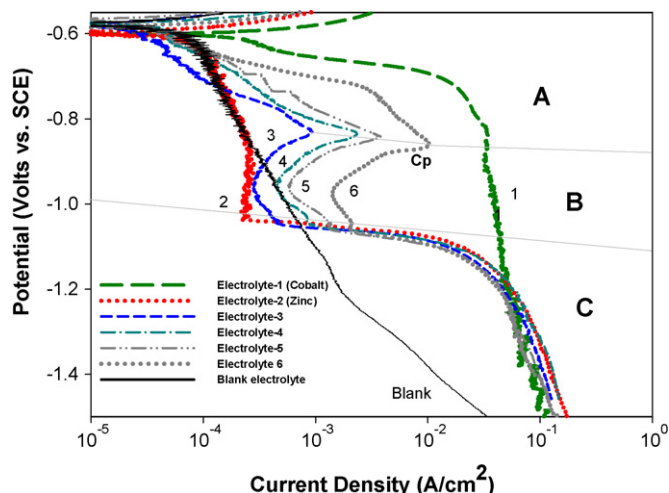


Fig. 2. Cathodic potentiodynamic electrodeposition on steel substrate. The curves show changes in the deposition behavior with the variation in concentration of Co^{2+} in the electrolyte: (curve 1) 100% Co, (curve 2) 100% Zn, (curve 3) 27.6% Co, (curve 4) 36.4% Co, (curve 5) 40% Co and (curve 6) 44% Co. The polarization is carried out at 35°C , $\text{pH } 3.5$ at a scan rate of 1 mV/s .

as mentioned in previous section. The polarization curves from the blank electrolyte (with and without N_2 purging) are plotted to identify the contribution of hydrogen and oxygen reduction reactions from the blank electrolyte during actual metallic deposition. It is shown that the current density increases with the increase in cathodic potential mainly due to the reduction reaction of H^+ ions that result in H_2 evolution. However, the comparison of both curves shows some contribution of oxygen reduction reaction in the initial part of the curves. The hydrogen evolution increases with the increase in cathodic potentials, also observed by the formation of tiny bubbles at the cathode surface area.

Fig. 2 shows the cathodic potentiodynamic polarization curves for zinc, cobalt and ZnCo alloys (electrolytes 1–6) on steel substrate from their respective plating solutions, as given in Table 1, under the operating conditions mentioned above. In case of pure zinc, at potentials below the rest potential (-0.59 V) till -1.04 V the current density does not increase the same way as it did for blank electrolyte. As the potential reaches -1.05 V , the current density increases abruptly and corresponds to the onset of zinc deposition. The current density continues to increase until it reaches -1.25 V and beyond which a limiting stage appears. The limiting current density is found to increase with the increase in temperature and stirring rate of the electrolyte (not shown here). In case of cobalt, the electrodeposition starts at about -0.60 V in the given electrolyte. The current density increases markedly below -0.60 V and continues to do so until it reaches -0.82 V . At this potential the current density does not increase further and the deposition reaches its limiting stage.

In case of cathodic potentiodynamic polarization for the Zn–Co alloys (curves 3–6), the curves follow pure cobalt curve in region “A” beyond the rest potential. Nevertheless, the current density in region A is suppressed and the curves deviate from the cobalt curve with the increase of Zn^{2+} ions in electrolytes and with increasing cathodic potential. The presence of Zn^{2+} ions in electrolyte appears to be responsible for the suppression of

current density. With the further increase in potential, as shown in curves 3–6, a critical potential (C_p) is observed. Below C_p , the current density decreases abruptly (marked as region B) and the deposition in this region suffers from severe inhibition, as shown by the drop in cathodic current density. With the increase in Zn^{2+}/Co^{2+} ratio in electrolyte the current density corresponding to C_p decreases and the Zn–Co alloy deposition curves also shift further away from the Co deposition curve in both regions A and B. The current density continues to decrease till the potential reaches -1.04 V to -1.05 V for bath 3–6, respectively, at which the current density increases distinctly (marked as region C). This sudden rise in current density indicates that whatever was the cause of mitigation is removed and the current density increases till -1.25 V followed by a region of limiting current density.

3.2. Electrodeposition and analysis in three regions

In Fig. 2, during potentiodynamic polarization in Zn–Co electrolyte, three regions are identified. In this section, the potentiostatic deposition is performed in all the three regions and the obtained deposits are analyzed by anodic stripping method. One of the reasons of carrying out the potentiostatic deposition in all three regions is to rule out the influence of any initially deposited Co layer on the substrate formed during the potentiodynamic cathodic polarization, as shown in Fig. 2. While for anodic stripping, the coatings in the mentioned three regions were obtained for 15–20 s of potentiostatic deposition in order to obtain a thin layer for a good and fast qualitative analysis with distinctive peaks. The morphology and composition of the deposits are analyzed by using SEM/EDX analysis.

3.2.1. Potentiostatic deposition and anodic stripping curves in region A

Fig. 3 shows the potentiostatic deposition curves at -0.78 V, in the region marked as “A” in Fig. 2, for electrolytes 3–5. The potentiostatic deposition is carried out for 5 min at 35°C under the given conditions. In case of curve 3 the current den-

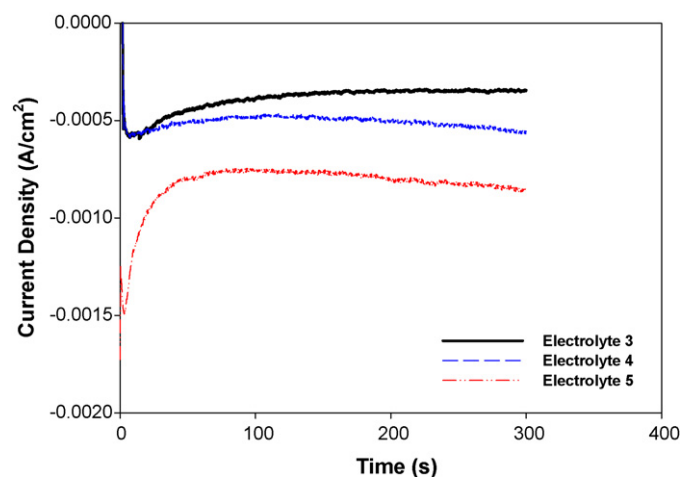


Fig. 3. Potentiostatic electrodeposition from electrolytes 3–5 electrodeposited at -0.78 V (region A). The deposition was carried out at 35°C , at a pH of 3.5 and stirring rate of 350 rpm.

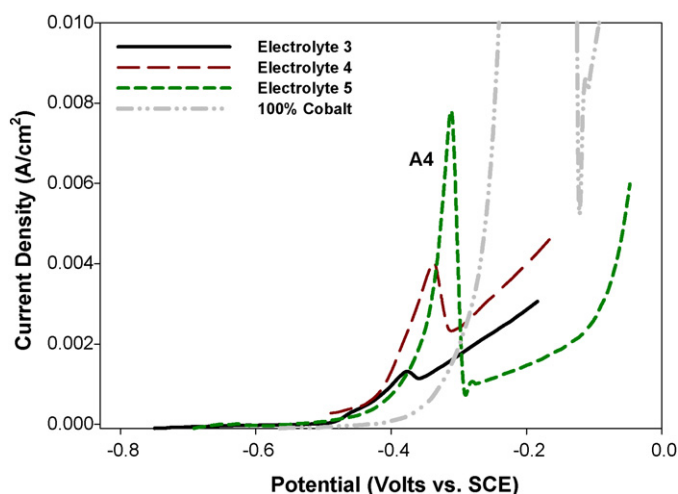


Fig. 4. In situ anodic stripping at a scan rate 10 mV/s of ZnCo alloy electrodeposited from electrolytes 1, 3, 4 and 5 at -0.78 V after deposition for 20 s at 35°C .

sity increases rapidly at the onset of the test and then decreases steadily over a longer period of time. In case of curves 4 and 5 the deposition seems to be time dependent and increases rapidly in the beginning but at a decreased rate over a longer period of time. The current density increases with the increase in Co^{2+} concentrations in the electrolyte but in general the current density values are very low in this potential region A (i.e. 0.0003 – 0.001 A/cm²).

The in situ anodic stripping results, shown in Fig. 4, are performed on deposits obtained after 20 s of potentiostatic deposition. The purpose of anodic stripping is to find out the role of zinc in causing inhibition of the deposition process. The deposits are stripped anodically right after the deposition under the same conditions in order to verify the findings shown in Fig. 3 and to see what phases are obtained in the deposits at certain potentials. The anodic peak related to pure cobalt is observed at -0.17 V, a potential value similar to that found in previous research [37]. The stripping peaks A_4 , corresponding to highly Co-enriched phase, have shifted towards more negative potential than pure Co peak and shift further away with the increase of Zn^{2+}/Co^{2+} ratio in electrolytes. It is shown that for the same duration of deposition the peaks vary in heights and increase with the increase of Co^{2+}/Zn^{2+} ratio in the electrolytes.

3.2.2. Morphology and composition of the deposits in region A

The composition analysis of deposits is done by EDX and the results are shown in Fig. 5A. The wt% cobalt in the deposit increases with the increase of Co^{2+} concentration in the electrolyte. The composition of the deposits indicates a relatively higher wt% of Co (91–97% Co) than wt% of Co^{2+} in the electrolyte. It also verifies the presence of Zn (3–9%) in the deposit. The SEM micrograph of Zn–Co alloy deposit obtained potentiostatically at -0.78 V from bath 5 is shown in Fig. 5B. The EDX composition analysis reveals that the deposit contains 6% of Zn and the rest is cobalt. The composition can be related to α -phase of Zn–Co alloy that has a maximum Zn solubility of 30%, as reported in literature [22].

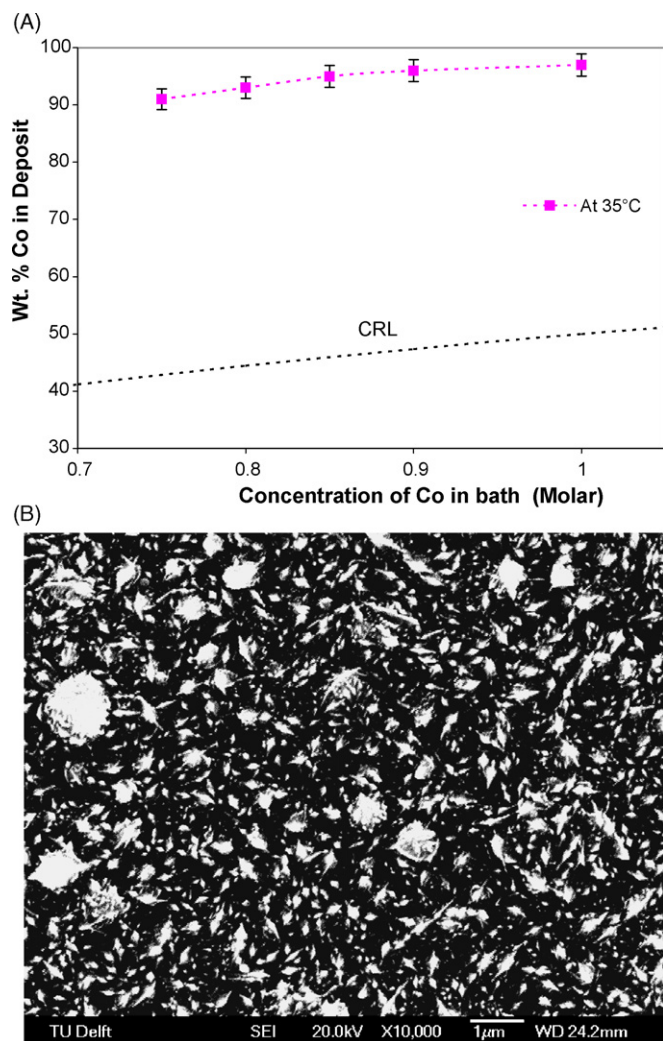


Fig. 5. (A) Variation of Co content in the Zn–Co alloy deposit as a function of variation in concentration of Co in electrolyte deposited at -0.78 V at 35°C , determined by EDX. The amount of Zn in electrolyte is 1.1 M. (B) Micrograph of deposit obtained from electrolyte 5 at 35°C at -0.78 V. Deposit contains $\sim 6\%$ Zn.

3.2.3. Potentiostatic deposition and anodic stripping in region B

In this section, the deposition behavior in region B is considered, where the current density decreases distinctly, as shown in Fig. 2. In order to observe the deposition behavior in region B the potentiostatic deposition of Zn–Co alloys is carried out from electrolyte 3–5 at -0.94 V at 35°C , as shown in Fig. 6. It is shown that the current density increases sharply during the first few seconds followed by a reduction and then it decreases gradually at a lower rate over the rest of deposition time. It is also noticeable that the current density increases with the increase of the cobalt concentration in the electrolyte but in general the deposition rate is rather low.

Fig. 7 shows the anodic stripping of the deposits obtained potentiostatically during 20 s. It is noteworthy that only one peak is visible, which increases in height with the increase in Co^{2+} concentration in the electrolyte. In addition, it is also shown that the alloys peaks shift towards pure cobalt (more positive) with the decrease in Zn^{2+} ratio in electrolytes.

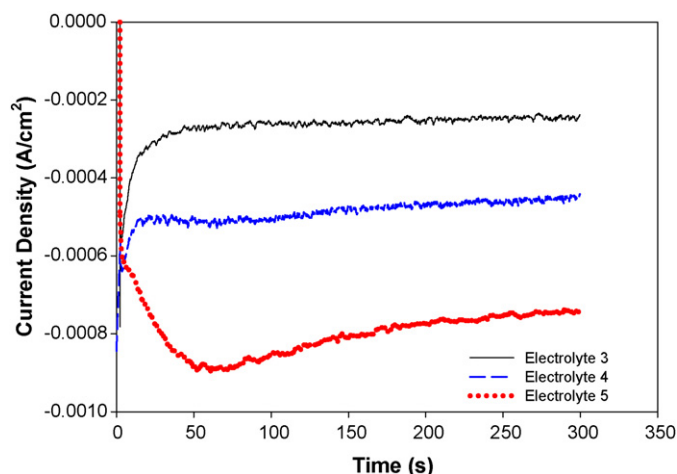


Fig. 6. Potentiostatic electrodeposition from electrolytes 3–5 electrodeposited at -0.94 V (region B). The deposition was carried out at 35°C .

3.2.4. Morphology and composition of deposits in region B

Fig. 8 shows the SEM micrograph of the deposit obtained at -0.94 V, where the cathodic deposition is severely inhibited, as shown in Figs. 2 and 6. The deposit, after 3 h of deposition, is very thin and EDX composition analysis reveals approximately 3–5% Zn in deposit and the rest is cobalt.

3.2.5. Electrodeposition in region C

In this section, the deposition behavior in region C is considered, where the current density increases markedly, as shown in Fig. 2. In order to explain the deposition behavior in region C, the composition of Co in Zn–Co alloy deposits (analyzed by EDX) versus Co^{2+} concentration in electrolyte is plotted in Fig. 9. The deposits are obtained potentiostatically at -1.1 V and at 35°C from the electrolytes containing various molar concentration of Co^{2+} . It is found that the amount of cobalt in deposit increases with the increase of Co^{2+} concentration in the electrolyte but the compositions of alloys remain always lower than the composition reference line (CRL), defined as:

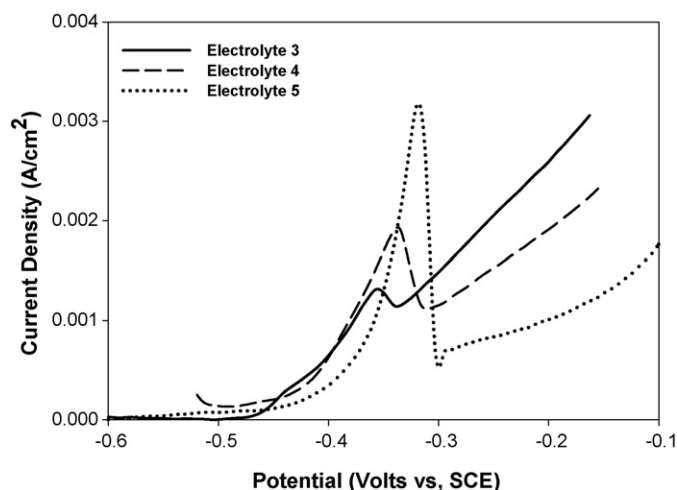


Fig. 7. In situ anodic stripping at a scan rate 10 mV/s of ZnCo alloy electrodeposited from electrolytes 3–5 at -0.94 V after deposition for 15 s at 35°C .

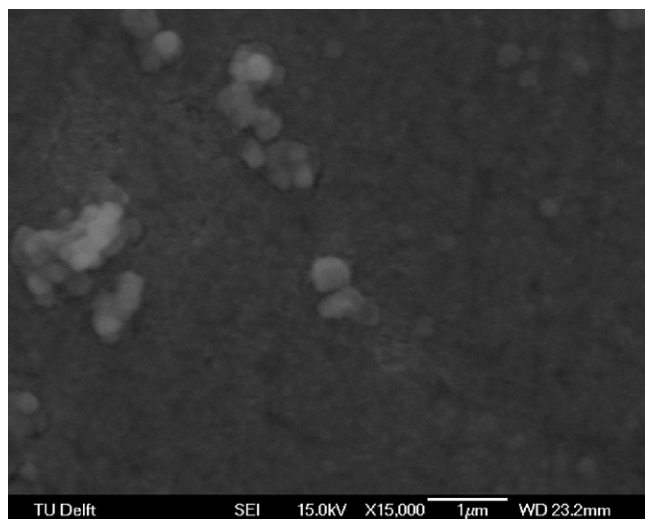


Fig. 8. Micrograph of deposit obtained from electrolyte 5 at 35 °C at -0.94 V. Deposit contains ~93% Co and the rest is zinc.

$$\text{CRL} = \frac{c(\text{Co}^{2+})}{[c(\text{Co}^{2+}) + \text{Zn}^{2+}]} \quad (1)$$

where $c(\text{Co}^{2+})$ and $c(\text{Zn}^{2+})$ are the concentrations of cobalt and zinc in electrolytes.

It is also noteworthy that a significant increase in wt% Co in deposit occurs beyond 0.8 M Co in the electrolyte. In case of electrolyte 7, the wt% Co in the deposit becomes very high and the composition becomes closer to the CRL.

3.2.6. Potentiostatic deposition and anodic stripping curves in region C

Fig. 10 shows the potentiostatic deposition curves at -1.1 V, in the region marked as “C” in Fig. 2, for electrolytes 3–5. The current density increases rapidly during the first few seconds and then increases gradually over the rest of deposition period of time. As shown in Fig. 10, the curves in general show a higher deposition rate as compared to regions A and B in

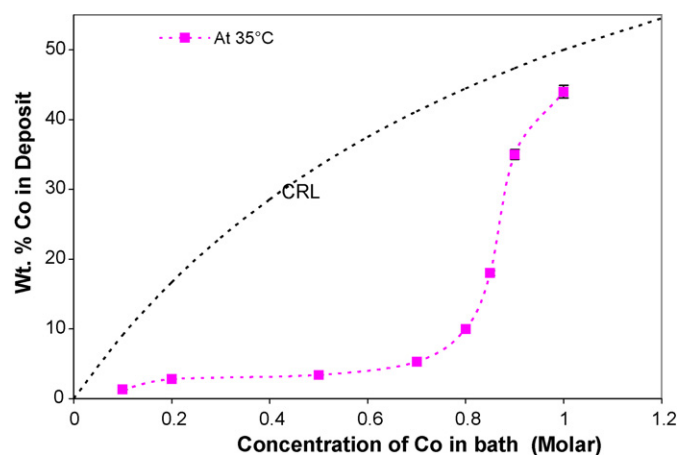


Fig. 9. Variation of Co content in the Zn–Co alloy deposit as a function of variation in concentration of Co in electrolyte deposited at -1.1 V at constant conditions of 35 °C. The amount of Zn in electrolyte is 1.1 M and the composition was determined by EDX.

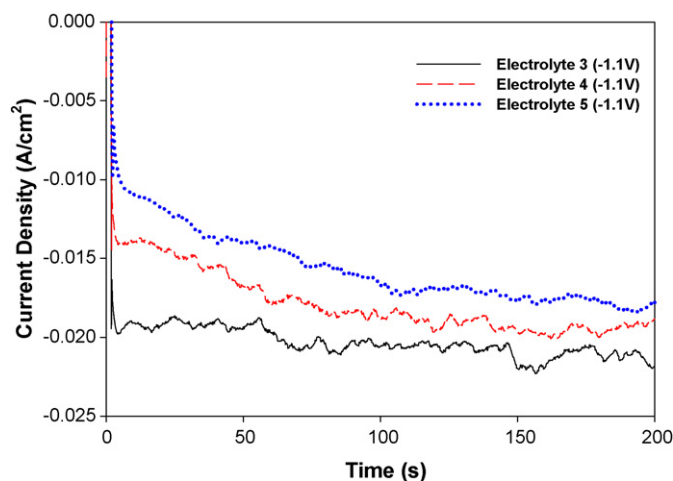


Fig. 10. Potentiostatic electrodeposition from electrolytes 3–5 electrodeposited at -1.1 V (region C). The deposition was carried out at 35 °C.

terms of current density. However in contrast to the findings of Fig. 3, it is evident that an increase of Co^{2+} concentration in electrolyte results in a reduction of cathodic current density. On the other hand an increase of $\text{Zn}^{2+}/\text{Co}^{2+}$ ratio in the electrolyte results in an increase in the deposition rate in this region.

The anodic stripping curves shown in Fig. 11 indicates a shift in all peaks towards more positive potential and also Co enriched peaks as a result of increase in $\text{Co}^{2+}/\text{Zn}^{2+}$ ratio in the electrolytes. It is also shown that the anodic stripping starts with the dissolution of Zn-enriched phase (as shown by peak A₁) and is followed by Zn–Co phases relatively richer in Co (as shown by peak A₂). After dissolution of phase corresponding to peak A₂, the highly Co-enriched peaks A₃ and A₄ are visible. It is worth noticing that the peak A₃ is visible for curve corresponding to electrolyte 3 while it appears as a left shoulder of peak A₄ for electrolytes 4 and 5. However, the peak A₄ is only noticeable for electrolyte 4 and 5 and is not found for electrolyte 3. The peaks heights of the anodic stripping curves,

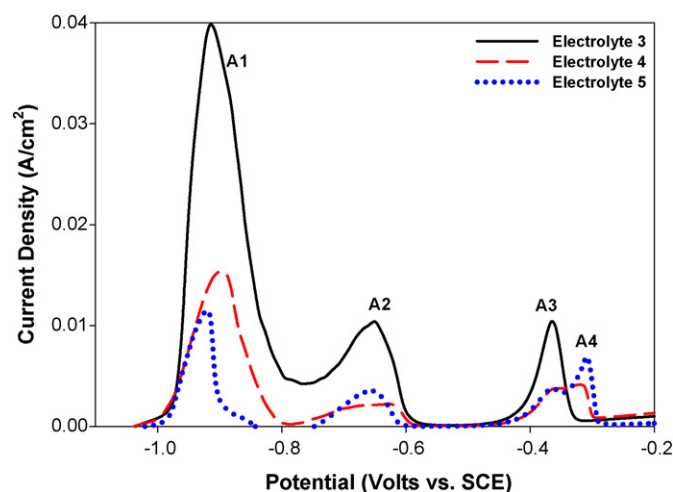


Fig. 11. In situ anodic stripping at a scan rate 10 mV/s of ZnCo alloy electrodeposited from electrolytes 3–5 at -1.1 V at 35 °C.

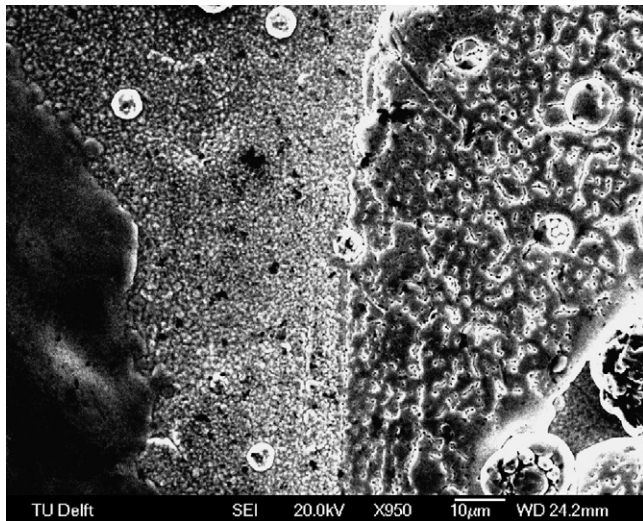


Fig. 12. Micrograph of deposit obtained from electrolyte 5 at 35 °C at -1.1 V. Deposit contains 18% Co.

shown in Fig. 11, verify the lessening of deposition with the increase of Co^{2+} concentration in the electrolyte, as shown in Fig. 10.

3.2.7. Morphology and composition of deposits in region C

The deposit obtained from electrolyte 5 at -1.1 V and at 35 °C is shown by the micrograph in Fig. 12. The EDX analysis of deposit shows that it contains approximately 18 wt% Co which is far less than CRL. The EDX analysis reveals the presence of more than two areas with different compositions at the surface, which is also confirmed by the emergence of several peaks as shown by anodic stripping in Fig. 11. Fig. 13 shows the micrograph of Zn–Co alloy deposited from electrolyte 7 at -1.1 V and some micro cracks are also visible at the surface. The composition analysis shows more than 42% Co in alloys, which is still less than CRL.

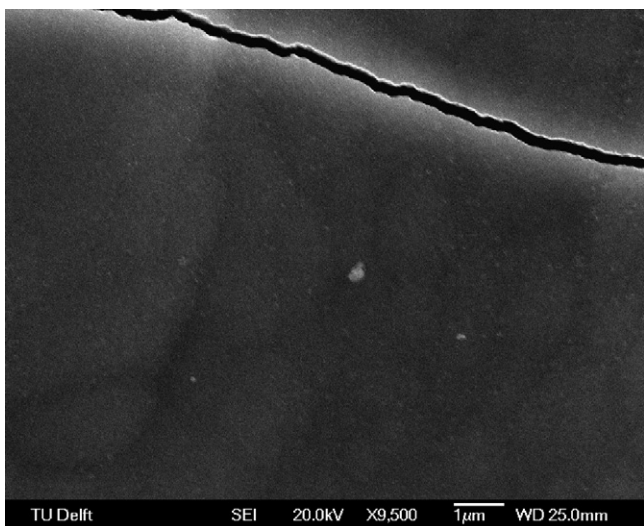


Fig. 13. Micrograph of deposit obtained from electrolyte 7 at 35 °C at -1.1 V. The deposit contains 42% Co.

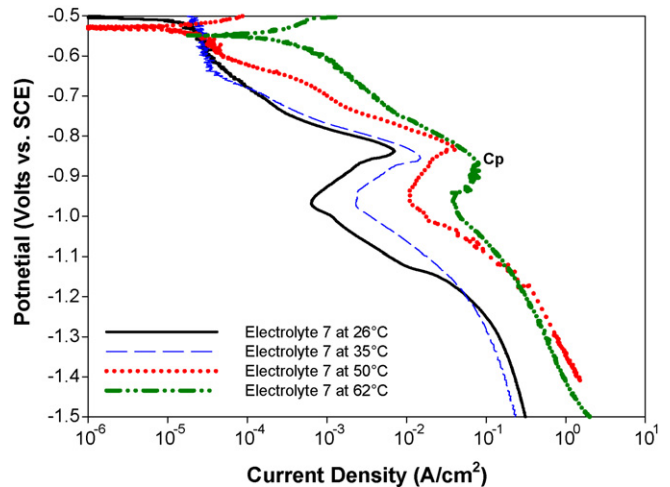


Fig. 14. Cathodic potentiodynamic polarization curves showing the effect of temperature on the electrodeposition behavior. The curves are obtained from bath 7 at pH 3.5 and at constant stirring of 350 rpm.

3.3. Effects of temperature on the deposition behavior

In this section, the effect of an increase in temperature on the anomalism is investigated. Fig. 14 shows the potentiodynamic polarization curves for electrolyte 7 and shows the effect of temperature (26–62 °C) on the deposition behavior. It is shown that the current density corresponding to C_p increases with the increase in electrolyte temperature. It is also noteworthy that the region of severe inhibition though does not completely disappear but reduces with the increase in temperature, as shown by the comparison of the curves. The deposition rate in general increases and it appears that the cause of inhibition fades away with the increase in temperature.

3.4. Local pH measurement

In order to verify the HSM theory and to ascertain the formation of $\text{Zn}(\text{OH})_2$ at the cathode surface, the local pH measurement experiment was carried out. A significant raise in local pH (>5.0) can be related to the formation of $\text{Zn}(\text{OH})_2$ at the cathode. The experiment was carried out as stated in literature [14]

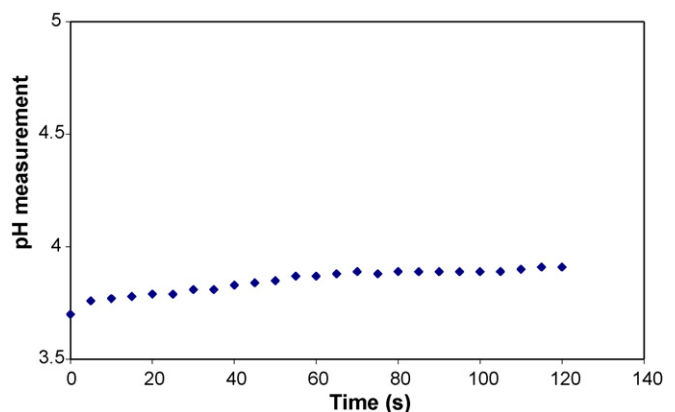


Fig. 15. The pH measurements at potentiostatic electrodeposition from electrolyte 6 at -1.1 V. The deposition was carried out at stirring rate of 350 rpm.

on a Pt mesh at room temperature. However, instead of using the rotating disc electrode the solution was stirred at 350 rpm. Fig. 15 shows the graph of pH change with time during potentiostatic electrodeposition from baths 6 at -1.1 V. During 2 min deposition time a deposit of approximately $2 \mu\text{m}$ was achieved. It is shown that during the potentiostatic electrodeposition the local pH value does not increase considerably from the initial value of 3.7.

4. Discussion

The electrodeposition of Zn–Co alloys is a complex process that involves inhibition and anomalism in different potential regions. It is divided into three potential regions, i.e. a normal deposition region A (positive to Zn deposition potential $E_{\text{Zn}}^0 = -1.05$ V versus SCE), an anomalous deposition region C (negative to E_{Zn}^0) and the region B located in between. A critical potential “Cp” is also reported here subsequent to region A for the first time in the polarization curves (to our knowledge) beyond which the deposition is sharply mitigated.

The deposition of Co starts around -0.6 V through nucleation at a few active sites and increase steadily with potential until -0.75 V mainly through growth mechanisms, also reported by other researchers [3,37,38]. In case of Zn deposition curve (between -0.8 and -1.04 V), the current density remains lower than that for blank electrolyte. It appears that addition of Zn^{2+} in electrolyte has suppressed the other reduction reactions (mainly H^+ reduction). This suppression of H^+ reduction prior to -1.05 V is related to the UPD of zinc on steel substrate, as the UPD of Zn has previously been reported [27–35] on several substrates including steels. It is known that Zn has a lower exchange current density for H^+ reduction (i.e. in the order of $10^{-10.5}$ A/cm²) as compared to Fe (approximately $10^{-5.5}$ A/cm²) [25]. Therefore the low cathodic current density recorded in case of pure Zn deposition on steel substrate prior to -1.04 V is due to UPD of Zn, which suppressed hydrogen evolution reaction (HER).

The mechanisms related to the deposition of Zn–Co alloys, on steel substrates, in the three regions A–C can be explained as follows.

The curves in region A, prior to Cp, indicate that the deposition rate increases steadily with the increase in cathodic potential. However, the curves are suppressed compared to the pure Co curve and Cp shift towards more positive potentials due to increase of $\text{Zn}^{2+}/\text{Co}^{2+}$ ratio in the electrolytes. During deposition in region B, i.e. below Cp, a pronounced inhibition in deposition and an abrupt decrease in current density occur. The anodic stripping curves, for both region A and B verified the presence of Co-enriched Zn–Co alloy phase, usually referred as α phase according to some researchers [22], which is located at potentials more negative to pure cobalt. It is illustrated that the peaks shift to further negative values and decrease in heights with the increase of Zn^{2+} ratio in the electrolytes. The EDX analysis of deposits obtained in regions A and B confirms the presence of small amount (approximately 5%) of Zn in the deposit. The microstructure is in agreement with the findings of some other researchers [3,35]. In principle, the addition of zinc

in the deposit at potentials positive to $E_{\text{Zn}}^0 = -1.05$ V is only possible through UPD mechanism. The potential at which UPD takes place is defined by Kolb and Gerischer [39] by a relationship, i.e. $\Delta E = 0.5 \Delta\phi$, where ΔE is the underpotential shift and $\Delta\phi$ is the difference in work function values between the foreign metallic substrate and the electrodeposited metal. The UPD is expected when the work function value ϕ of the deposited metal is smaller than that of the substrate metal. Therefore, considering ϕ , the UPD of Zn on steel and Co is not unexpected and UPD interaction of Zn with steel and Co can occur at potentials more positive than the Nernst zinc deposition potential [23,24,31].

It is considered that in both regions A and B the deposition of Co takes place via progressive nucleation and three dimensional growth mechanisms. In the presence of Zn the nucleation rate becomes much lower due to UPD of Zn than in electrolyte without any Zn [41]. The sub-monolayer Zn deposited on the substrate inhibits the formation of clusters or nuclei of Co on the substrate hereby limiting the space available for Co deposition. Furthermore, a Co cluster that has the critical size for spontaneous growth resembles bulk Co and UPD of Zn on Co cluster also occurs and inhibits it further from growth. This inhibition of Co at the cluster growth stage due to the interaction with zinc is also suggested by some authors [23]. In addition, the presence of a higher amount of Zn^{2+} ions in the cathodic diffusion layer may also interfere with the replenishment of Co^{2+} ions in the cathodic layer.

It is realized that it is difficult to determine the deposition kinetics of Zn and Co at higher overpotential (in region C and > -1.2 V) due to complexity of polarization curves in that region and lack of information (i.e. not covered in this paper). However, some researchers have calculated and compared the deposition kinetics of both Zn and Co at equilibrium and various concentrations of electrolytes [18,20,23,24,40] and concluded that Zn has faster deposition kinetics than Co. The anomalism found in region C is scrutinized under both deposition kinetics and HSM theories.

On the basis of former theory, as there exists a competition between Zn^{2+} and Co^{2+} to occupy the active sites on the substrate, Zn^{2+} deposits preferentially due to its faster deposition kinetics as compared to cobalt. This is supported by the potentiostatic deposition, in which an increase of Co^{2+} concentration in electrolyte though resulted in a comparatively higher amount of cobalt in deposits but reduced the cathodic current density for deposition. The higher Co (wt%) in deposit with the increase of Co^{2+} concentration in the electrolyte is attributed to an increase in Co^{2+} ions in cathodic layer while due to slower deposition kinetics it lowers the overall deposition rate of the alloy. The increase of $\text{Co}^{2+}/\text{Zn}^{2+}$ ratios in electrolyte assists in overcoming the so-called anomalism to a great extent. On the contrary, the increase of $\text{Zn}^{2+}/\text{Co}^{2+}$ ratio in electrolyte results in a higher deposition rate and more Zn in deposit. This may be attributed to an increase in Zn^{2+} ions (that has faster deposition kinetics) in the cathodic layer and as a result elevates the overall deposition rate of alloy.

It is found that the increase in temperature assists in increasing the deposition rate of Co and overcoming the anomalism during deposition. It may be attributed to the increase in depo-

sition kinetics of Co at elevated temperature that results in increasing Co^{2+} ions in the cathodic layer and faster replenishment during deposition. It is noteworthy that with the increase in temperature the onset of region C shifts to more positive potentials with higher amount of cobalt in the deposit. However, it is also noticeable that the regions A and B though reduced did not disappear with the rise in temperature, where UPD is considered to play role, as discussed earlier.

The local pH measurement shows that the pH does not change significantly from the initial pH to form $\text{Zn}(\text{OH})_2$. Moreover, the 30 g/L of Boric acid is added to the bath, which is reported advantageous in preventing hydroxide from precipitation at the cathode [1]. Therefore, the HSM theory does not seem likely to explain the anomalism mechanism in any of the three regions as it does not explain the deposition of small amount of Zn along with Co in region A and B, the presence of Cp and the occurrence of severe mitigation after Cp in region B. Moreover, the HSM theory also does not explain the increase in Co (wt%) in deposit at higher temperature and from electrolyte containing higher $\text{Co}^{2+}/\text{Zn}^{2+}$ ratios.

5. Conclusions

It is usually considered that the inhibition of Fe-group metals occur subsequent to Nernst equilibrium potential corresponding to Zn. But it is noticed in this investigation that inhibition occurs a lot earlier than that. However, there are different reasons for inhibition or anomalism during deposition in different potential regions. In regions A and B (usually considered the normal deposition region), the difference of work function values $\Delta\phi$ between the two metals (Zn/Fe or Zn/Co) causes UPD of Zn, which results in suppression of Co deposition and hydrogen reduction. The zinc UPD results not only in suppression of Co but also the thickness of deposit. In region "A", the Co-enriched phase of Co–Zn alloy is noticed during anodic stripping. A critical potential is also noticed in this investigation. The inhibition becomes severe subsequent to critical potential, which is due to UPD of Zn on discharged Co^{2+} or developed Co clusters at both the nucleation and growth stage. With an increase of $\text{Zn}^{2+}/\text{Co}^{2+}$ ratio in the bath the critical potential shifts upwards (towards positive potential) and as a result the percentage of Co in deposit also decreases prior to the critical potential. It is found that deposition at high temperature in this region assists in increasing the deposition rate but the critical potential and the inhibition range does not completely disappear. In the potential region C, cathodic to Nernst equilibrium potential for Zn (well known as the anomalous region), another mode of inhibition takes place during codeposition that results in a higher amount of Zn as compared to Co. In this anomalous codeposition, the faster deposition kinetics of Zn as compared to that of Co is considered responsible. It is found that increasing the $\text{Co}^{2+}/\text{Zn}^{2+}$ ratio and operating temperature of the electrolyte assist in overcoming the anomalism. It is also found that when the initial pH

is approximately 3.7, the local pH at the cathode surface during deposition does not rise high enough to form $\text{Zn}(\text{OH})_2$. Therefore, the HSM theory does not seem to play a role in anomalous codeposition of Zn–Co alloy.

References

- [1] A. Brenner, *Electrodeposition of Alloys*, vol. 2, Academic Press, New York, 1963, p. 194.
- [2] H. Dahms, I.M. Croll, *J. Electrochem. Soc.* 112 (1965) 771.
- [3] M. Yunus, C. Capel-Boute, C. Decroly, *Electrochim. Acta.* 10 (1965) 885.
- [4] J. Mindowicz, C. Capel-Boute, C. Decroly, *Electrochim. Acta* Vol.10 (1965) 91.
- [5] K. Higashi, H. Fukushima, T. Urakawa, T. Adaniya, K. Matsudo, *J. Electrochem. Soc.* 128 (1981) 2081.
- [6] H. Fukushima, T. Akiyama, K. Higashi, R. Kammel, M. Karimkhani, *Metal* 44 (1990) 754.
- [7] T. Akiyama, H. Fukushima, *ISIJ Int.* 32 (1992) 787.
- [8] H. Fukushima, T. Akiyama, M. Yano, T. Ishikawa, R. Kammel, *ISIJ Int.* 33 (1993) 1009.
- [9] T. Tsuru, S. Kobayashi, T. Akiyama, H. Fukushima, S.K. Gogia, R. Kammel, *J. Appl. Electrochem.* 27 (1997) 209.
- [10] H. Yan, J. Downes, P.J. Boden, S.J. Harris, *J. Electrochem. Soc.* 143 (1996) 1577.
- [11] H. Deligianni, L.T. Romankiw, *IBM J. Res. Dev.* 37 (1993) 85.
- [12] S. Hessami, C.W. Tobias, *J. Electrochem. Soc.* 128 (1989) 838.
- [13] S.L. Diaz, O.R. Mattos, O.E. Barcia, F.J. Miranda, *Electrochim. Acta* 47 (2002) 4091.
- [14] V.G. Rovez, N.V. Gudin, *Trans. IMF* 74 (5) (1996) 153.
- [15] E. Gomez, E. Valles, *J. Electroanal. Chem.* 397 (1995) 177.
- [16] E. Chassaing, R. Wiart, *Electrochim. Acta* 37 (3) (1992) 545.
- [17] F.J. Fabri Miranda, O.E. Barcia, O.R. Mattos, R. Wiart, *J. Electrochem. Soc.* 144 (1997) 3441.
- [18] R. Fratesi, G. Roventi, *Mater. Chem. Phys.* 23 (1989) 529.
- [19] R. Fratesi, G. Roventi, *J. Appl. Electrochem.* 22 (7) (1992) 657.
- [20] M. Mathias, T. Chapman, *J. Electrochem. Soc.* 134 (1987) 1408.
- [21] M. Mathias, T. Chapman, *J. Electrochem. Soc.* 137 (1990) 102.
- [22] R. Fratesi, G. Roventi, G. Giuliani, C.R. Tomachuk, *J. Appl. Electrochem.* 27 (1997) 1088.
- [23] M. Ohba, Z. Panossian, P. Camargo, *Trans. IMF* 83 (4) (2005) 199.
- [24] M. Ohba, Z. Panossian, P. Camargo, *Trans. IMF* 84 (6) (2006) 320.
- [25] Z. Li, J. Cai, S. Zhou, *Trans. IMF* 77 (4) (1999) 149.
- [26] S. Swathirajan, *J. Electroanal. Chem.* 221 (1987) 211.
- [27] M.J. Nicol, H.I. Philip, *J. Electroanal. Chem.* 70 (1976) 233.
- [28] J.H.O.J. Wijenberg, J.T. Stevels, J.H.W. De Wit, *Electrochim. Acta* 43 (7) (1997) 649.
- [29] T. Ohtsuka, A. Komori, *Electrochim. Acta* 43 (21/22) (1998) 3269.
- [30] P.Y. Chen, I.-W. Sun, *Electrochim. Acta* 46 (2001) 1169.
- [31] J.-F. Hung, I.-W. Sun, *J. Electrochem. Soc.* 151 (1) (2004) C8.
- [32] J. Vaes, J. Fransear, J.P. Celis, *J. Electrochem. Soc.* 149 (11) (2002) C567.
- [33] D.M. Kolb, M. Przasnyski, H. Gerischer, *J. Electroanal. Chem.* 54 (1974) 25.
- [34] J. Dogel, W. Freyland, *Phys. Chem. Chem. Phys.* 5 (2003) 2484.
- [35] J.O.M. Bockris, S.U.M. Khan, *Surface Electrochemistry*, 376, Plenum Press, New York, 1993, Chapter 3.
- [36] Y. Fujiwara, H. Enomoto, *J. Electrochem. Soc.* 147 (5) (2000) 1840.
- [37] M. Alcalá, M. Gomez, E. Valles, *J. Electroanal. Chem.* 370 (1994) 73.
- [38] G. Roventi, T. Bellezze, R. Fratesi, *Electrochim. Acta* 51 (2006) 2691.
- [39] D.M. Kolb, M. Przasnyski, H. Gerischer, *J. Electroanal. Chem.* 54 (25) (1974).
- [40] J.M. West, *Corrosion*, vol. 38, Newnes–Butterworth, 1976 (chapter 21).
- [41] Cao, Yang, Ph.D., Columbia University, 2000.